Pt- and Pd-Modified Transition Metal Nitrides Catalysts for the Hydrogen Evolution Reaction

Journal:	*Physical Chemistry Chemical Physics*
Manuscript ID	CP-ART-02-2022-000792.R1
Article Type:	Paper
Date Submitted by the Author:	24-Mar-2022
Complete List of Authors:	Ologunagba, Damilola; Florida A&M University, Physics Kattel, Shyam; Florida A&M University, Physics

Pt- and Pd-Modified Transition Metal Nitrides Catalysts for the Hydrogen Evolution Reaction

Damilola Ologunagba, and Shyam Kattel*

Department of Physics, Florida A&M University

Tallahassee, FL 32307 USA

*Corresponding author: shyam.kattel@famu.edu

ABSTRACT

Hydrogen production via the electrochemical splitting of water using renewable electricity represents a promising strategy. Currently, Platinum group metals (PGM) are the best performing hydrogen evolution reaction (HER) catalysts. Thus, the design of non-PGM or low-loading PGM catalysts is essential for the commercial development of hydrogen generation technologies via the electrochemical splitting of water. Here, we employed density functional theory (DFT) calculations to explore Pt/Pd modified transition metal nitrides (TMNs) as low-cost HER catalysts. Our calculations show that Pt/Pd binds strongly with TM on TMN(111) surfaces, leading to the formation of stable Pt/Pd-monolayer (ML)-TMN(111) structures. Furthermore, our calculated hydrogen binding energy (HBE) demonstrates that Pt/MnN, Pt/TiN, Pt/FeN, Pt/VN, Pt/HfN, Pd/FeN, Pd/TaN, Pd/NbN, Pd/TiN, Pd/HfN, Pd/MnN, Pd/ScN, Pd/VN, and Pd/ZrN are promising candidates for HER with a low value of limiting potential (U_L) similar to that calculated on Pt(111).

Keywords: hydrogen evolution reaction, density functional theory, catalysts, free energy, limiting potential

1. INTRODUCTION

Hydrogen is an attractive alternative clean fuel.[1-3] However, currently, hydrogen is produced primarily via the catalytic reforming of hydrocarbons and alcohols using precious metals catalysts.[4,5] Such fossil fuel-based production of hydrogen is not sustainable and also energy-intensive as reforming is typically carried out at high temperatures.[6,7] In this regard, ambient condition electrochemical water splitting to produce hydrogen is appealing.[8-12] The electrochemical hydrogen production, when carried out using renewable electricity, represents a carbon neutral sustainable approach to producing hydrogen that can be used as a clean fuel.[13-16]

The electrochemical splitting of water consists of two half-reactions: hydrogen evolution reaction (HER) that occurs at the cathode, and oxygen evolution reaction (OER), which occurs at the anode. The HER at the cathode can proceed via Volmer-Heyrovsky or Volmer-Tafel mechanism[17–21]. In acidic solution, the elementary steps in HER are:[17]

$$H^+ + e^- \rightarrow H^* \quad \text{Volmer reaction}$$

$$H^* + H^+ + e^- \rightarrow H_2(g) + * \quad \text{Heyrovsky reaction}$$

$$H^* + H^* \rightarrow H_2(g) + * \quad \text{Tafel reaction}$$

Along the Volmer-Heyrovsky reaction pathway[22], the HER proceeds via the Volmer step followed by the Heyrovsky step. The Volmer step involves electron transfer to a proton to produce an adsorbed hydrogen (H*) on the catalyst surface. In the Heyrovsky step, electron-coupled proton transfer to H* produces $H_2(g)$. Along the Volmer-Tafel mechanism[22], the HER proceeds via the Volmer reaction described above to form surface-bound H*, and the Tafel step comprises the combination of two H* to produce $H_2(g)$.

Platinum group metals (PGM): Pt and Pd are the most stable and active catalysts for HER.[23-26] The high cost associated with PGM catalysts severely limits their large-scale application as HER catalysts.[27–29] Thus, reducing the loading of PGM in the catalyst design without compromising the activity is a promising strategy to develop low-cost and effective HER catalysts.[30-33] Core@shell architecture[34] consisting of low-cost core materials with thin PGM shell has been demonstrated to possess similar or even higher HER activity compared to PGM catalysts.[35] Several types of such catalysts structures: having less expensive core metals with Pt and Pd thin shell (ranging from monolayer to few atomic layers) have been studied for many electrochemical reactions, including the HER using experimental and theoretical methods.[22,36,37]

Transition metal carbides (TMCs), transition metal phosphides (TMPs), transition metal borides (TMBs), and transition metal nitrides (TMNs) have been explored as electrocatalysts for the HER.[38–62] Abghoui et al.[54] reported that TaN, HfN, MoN, and ScN catalyze HER at overpotentials between -0.09 V to -0.34 V. Peterson et al.[63] demonstrated that the activity of TMC catalysts is between low activities shown by early transition metals and the high activity shown by compounds of Pt/Pt-group metals. In addition to the above, TMPs have also been explored as potential catalysts for HER, including the phosphides of Co, Ni, and Fe.[11]

In this study, density functional theory (DFT) calculations are performed to study the HER on Pt and Pd monolayer on less expensive TMNs. A monolayer of Pt and Pd are optimized on the (111) surface of TMNs, and the DFT calculated hydrogen binding energy is used to predict a set of promising HER candidates. The results show that monolayer of Pt/MnN, Pt/FeN, Pd/TaN, Pd/NbN, Pd/TiN, Pd/HfN, Pd/MnN, Pd/ScN, Pd/VN, and Pd/ZrN are promising candidates for the HER.

2. COMPUTATIONAL METHODS

Periodic density functional theory (DFT)[64] calculations are performed using the Vienna Ab-Initio Simulation Package (VASP).[65,66] All DFT calculations are performed at the GGA level within the PAW-PW91[67,68] formalism and are spin-polarized.

The bulk structures of transition metal nitrides (TMNs) are modeled using the rock salt NaCl structure with an equal ratio of the transition metal (TM) and nitrogen (N). The unit cell of bulk TMNs contains four TM atoms and four N atoms. The DFT optimized bulk TMNs are used to cleave the TM terminated TMN(111) surfaces. The TMN(111) surfaces are modeled using a 4 bilayer (each containing one layer of TM and N) 3 × 3 surface slabs. A monolayer of Pt and Pd is placed on optimized TMN(111) surfaces to model Pt/Pd monolayer TMN [Pt/Pd-ML-TMN(111)] surfaces.

A vacuum of approximately 18 Å is added to the surface in the z-direction to minimize the artificial interactions between the slab and their periodic images. All calculations are carried out using a plane-wave basis set of 400 eV energy cutoff, and a 3 × 3 × 1 Monkhrost-Pack grid is used to carry out the Brillion zone integration[69]. Based on our experience,[70-72] the energy cutoff (400 eV) and k-point sampling (3 × 3 × 1) are large enough to obtain converged reaction energetics. During calculations, atoms in the bottom two layers are fixed while all other atoms are allowed to relax until the Hellman-Feynman force on each ion is less than 0.02 eV/Å.

The formation energy (E_f) of the bulk unit cell is calculated as:

$$E_f = \text{Energy(bulk unit cell)} - n^* \text{Energy(TM)} - n/2^*\text{Energy}(N_2) \qquad [1]$$

where Energy(bulk unit cell) is the total energy of TMN unit cell, Energy(TM) is the total energy of TM in the energetically most favorable bulk phase, Energy(N_2) is the total energy of N_2 molecule in the gas phase, and n is the number of TM and N atoms in TMN unit cell.

The surface energy of relaxed TMN(111) (σ^r) is calculated following the approach described in (Quesne et al.) [73]

$$\sigma^r = \frac{E_{relax} - nE_{bulk}}{A} - \sigma^u \qquad [2]$$

where the surface energy of unrelaxed TMN(111) (σ^u) is given by:

$$\frac{E_{slab} - nE_{bulk}}{2A} \qquad [3]$$

Here, E_{relax} is the energy of the relaxed slab, E_{bulk} is the energy of the bulk unit cell, A is the surface area of the slab, and n is the number of bulk unit cells required to form TMN(111) slabs.

The binding energy (BE) of adsorbate on the surface is calculated as:

$$\mathrm{BE(adsorbate)} = \mathrm{E(slab + adsorbate)} - \mathrm{E(slab)} - \mathrm{E(adsorbate)} \qquad [4]$$

where E(slab + adsorbate), E(slab), and E(adsorbate) are the total energies of the slab with adsorbate, clean slab, and adsorbate in the gas phase, respectively.

The free energy changes (ΔG) are calculated using the computational hydrogen electrode (CHE) model developed by Norskov and coworkers.[74] In this model, the chemical potential of a proton-electron pair ($H^+ + e^-$) is equal to half of the chemical potential of hydrogen gas molecule ($1/2\mu(H_2)$) at zero applied potential (U). Thus, the total chemical potential of the ($H^+ + e^-$) pair as a function of applied potential (U), at all temperature and pH values, can be calculated as $\mu(H^+ + e^-) = 1/2\mu(H_2(g)) - eU$.

The CHE model is employed at U = 0 V to construct the free energy diagrams (ΔG vs. reaction coordinates) of the HER. The Gibbs free energy (G) of a species is calculated as[74]

$$G = E + ZPE - TS \qquad [5]$$

Here, E is the total energy of a species obtained from DFT calculations, ZPE and S are the zero-point energy and entropy of a species, respectively, and T = 298.15 K.

Similar to the previous approach[75], a canonical ensemble (NVT) ab-initio molecular dynamics (AIMD) simulations on few select Pt, Pd/TMNs candidates are performed at 1000K for 5 ps using the VASP code.

3. RESULTS AND DISCUSSION

TMCs and TMNs typically exist in two common crystal phases: face centered cubic rocksalt and hexagonal close pack (HCP).[72,76-81]. In particular, many of these TMNs (e. g. NbN, VN, ZrN, RuN, TiN, CrN, CoN) in rocksalt structures have been synthesized in previous experimental studies.[82-87] Therefore, we focus on the HER activity of 3d-5d TMNs in rocksalt phase. TMNs in other bulk phases will be our interest in future studies. Firstly, DFT calculations are performed to compute the lattice constant and formation energies (E_fs) of 3d-5d TMNs in rocksalt (NaCl: space group = $Fm\overline{3}m$) bulk structure. The DFT calculated lattice constants in Figure 1 show a correlation between the DFT calculated lattice constants and atomic radii of TMs in TMNs (except for ZnN), indicating that the lattice constant of the bulk TMN is primarily determined by the size of TMs. The correlation observed between the DFT calculated lattice constants of TMNs and atomic radii of TMs suggests that an advanced machine learning (ML) scheme can be developed to fit the lattice constant with elemental properties of TMs as illustrated in our previous study.[88] Such a ML study, which requires sizeable dataset, will also help identify the most important feature relating to target property (lattice constant in this case). Our calculated E_fs in Table 1 show negative E_f for CrN, HfN, MnN, MoN, NbN, ScN, TaN, TiN, VN, YN, and ZrN and a small positive E_f for AgN, AuN, CuN, FeN, IrN, NiN, ReN, RhN, RuN, TcN, WN, and ZnN. The positive E_f indicates the thermodynamically unfavorable formation of AgN, CoN, CuN, FeN, ZnN, AuN, IrN, NiN, ReN, RhN, RuN, TcN, and WN. Therefore, these TMNs are not included in the subsequent discussion of the HER activity. Secondly, we calculated the surface energies of TM-terminated-TMN(111) surfaces, which represent the thermodynamically most stable facet of face centered cubic rocksalt phase. Furthermore, a strong interaction between the TM terminated surfaces of TMNs/TMCs and Pt/Pt is expected due to similar electronic structures of TMNs/TMCs and Pt/Pt leading to stable Pt/Pd overlayers.[82,89-91] The DFT calculated surface energies (Table 1) are all positive, except for

TcN, and are similar to those reported on transition metal carbides (TMCs).[73] TMCs have been successfully synthesized and studied as catalysts for thermo/electro-catalytic reactions.[92] The negative E_f of several of TMNs and their comparable surface energies of the (111) facets to TMCs counterpart suggest that TMNs represent a new set of materials worthy of further investigation for application in catalysis.

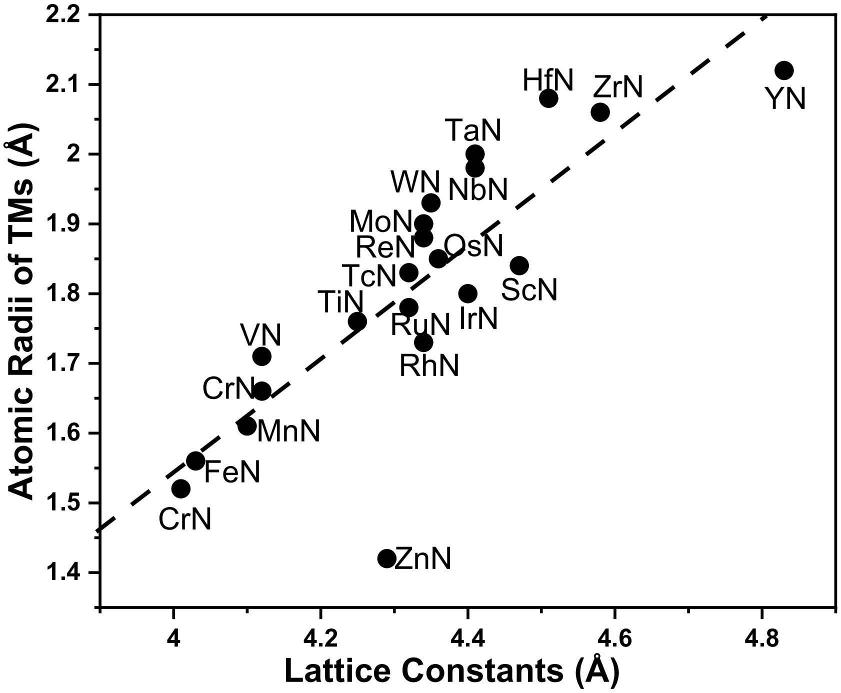

Figure 1. Plot showing the relationship between the atomic radii of TMs (Å) and their lattice constants (Å).

Table 1. Lattice constants (in Å) and Formation energies/atom (eV/atom) of bulk TMNs, and surface energies (Jm^{-2}) of TMN(111) surfaces.

TMNs	Lattice constant (Å)	E_f/atom (eV/atom)	Surface energies (Jm^{-2})
AgN	4.56	1.61	0.42
AuN	4.62	1.71	0.39
CoN	4.01	-	0.83
CrN	4.12	-0.39	-
CuN	4.17	0.99	0.79
FeN	4.03	0.19	0.88
HfN	4.51	-1.82	0.98
IrN	4.40	1.45	1.11

MnN	4.10	-0.28	0.94
MoN	4.34	-0.04	0.58
NbN	4.41	-1.04	0.63
NiN	4.07	0.58	0.76
ReN	4.34	1.00	0.39
RhN	4.34	0.91	0.59
RuN	4.32	0.88	0.57
ScN	4.47	-1.99	1.24
TaN	4.41	-0.91	0.62
TcN	4.32	0.51	-0.03
TiN	4.25	-1.74	1.26
VN	4.12	-1.02	0.91
WN	4.35	0.25	0.46
YN	4.83	-1.60	0.78
ZnN	4.29	0.66	0.79
ZrN	4.58	-1.74	0.96

Next, DFT calculations are performed to optimize a monolayer (ML) of Pt and Pd (9 Pt/Pd atoms) on the optimized TMN(111) surfaces. The Pt/Pd overlayer on TMN(111) mimics the TMN@Pt core@shell structure. This kind of architectures has been shown to reduce not only the precious metal loadings but also improve the catalytic performance for electrocatalytic reactions.[93-97] Pt/Pd atoms are placed on two different hollow sites (Figure 2) to obtain the most favorable Pt/Pd-ML-TMN(111) surfaces. The results indicate that Pt is more stable on hcp hollow site on CrN, HfN, and VN. In contrast, Pt is more favorably adsorbed on fcc hollow sites on CuN, FeN, MnN, and TiN. In addition, the results also show that the hcp hollow site is the energetically most favorable site for Pd on HfN, NbN, TaN, and ZrN. On the other hand, the fcc hollow site is the most favorable site for Pd on CrN, CuN, FeN, MnN, ScN, TiN, and ZnN. The most favorable Pt-ML-TMN(111) (i. e. Pt ML adsorbed at hcp hollow site on CrN, HfN, TaN, NbN, VN And fcc hollow site on CuN, FeN, TiN, ZnN) and Pd-ML-TMN(111) (i. e. Pd ML adsorbed at hcp hollow site on HfN, NbN, TaN, VN, ZrN and fcc hollow site on CuN, FeN, MnN, ScN, TiN, ZnN) are used for the calculations of H binding energy (HBE) as discussed below. It is observed that the

Pt/Pd forms a strong bond with the TM on TMN(111) as indicated by the negative binding energies listed in Figure 3. This is due to the similar electronic structure of TMNs and Pt/Pd.[98-101] Thus, Pt/Pd ML-TMN(111) structures are expected to be stable for their potential application as HER catalysts.

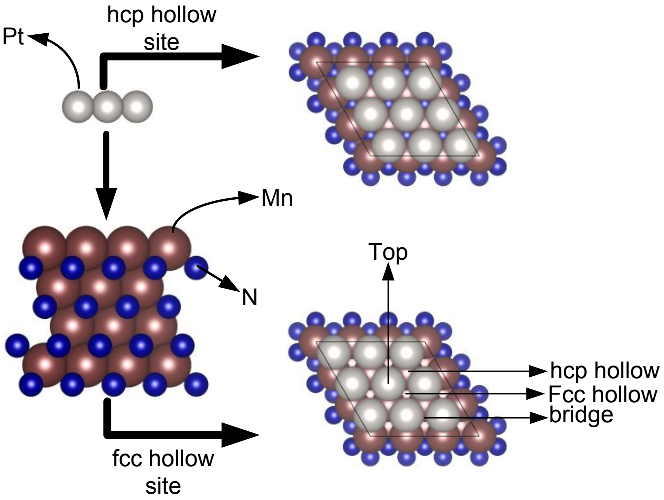

Figure 2. Schematics of how Pt/Pd-ML-TMN(111) are formed in the present study. TM (in TMNs): brown, Pt: gray, and N: blue

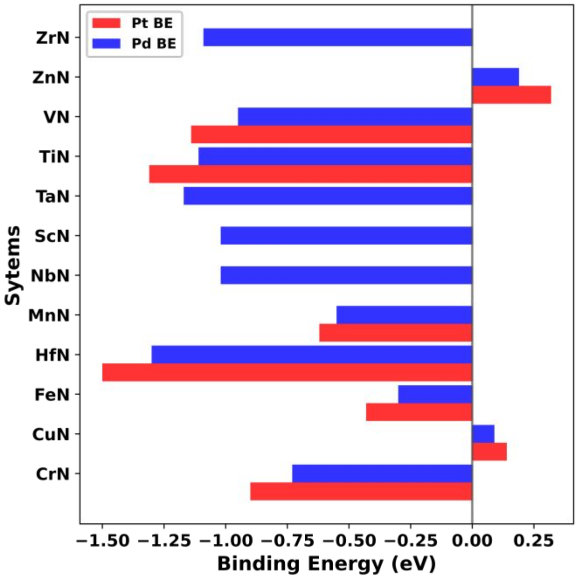

Figure 3. DFT calculated BE (in eV) per atom of Pt and Pd on TMN (111) surfaces.

The DFT optimized most stable structures of Pt/Pd-ML-TMN(111) are used to calculate the BEs of Pt and Pd on the TMN(111) surfaces. We found that Pt binds more strongly to CrN, FeN, HfNO, MnN, TiN, and VN compared to CuN and ZnN (Figure 3). On the other hand, Pd binds more strongly to CrN, FeN, HfN, MnN, NbN, ScN, TaN, TiN, VN, and ZrN compared to CuN and ZnN (Figure 3). Both Pt and Pd bind weekly to the CuN and ZnN surfaces compared to all other surfaces. The positive Pt/Pd binding energy on Pt/Pd ML on CuN and ZnN suggests that there is a weak interaction between Pt/Pd and Cu/Zn. This makes Pt/Pd more reactive as evidenced by the strong HBE (Figure 4). We notice that there is significant movement of Pt/Pd atoms during optimization leading to the formation of Pt/Pd cluster upon H adsorption, indicating adsorbate induced cluster formation. This behavior shows that Pt/Pd ML on MoN and YN are unstable; therefore, Pt/Pd-ML-MoN(111) and Pt/Pd-ML-YN(111) are excluded from the subsequent discussions of HER.

Sabatier's principle suggests that too strong HBE poisons the catalyst's surface and leaves no free sites for further H binding, whereas too weak HBE requires high overpotential for H adsorption.[102-104] Thus, an ideal catalyst should have an optimal HBE: neither too strong nor too weak. Previous experimental and theoretical studies have confirmed that the Gibbs free energy change of adsorbed hydrogen (ΔG_H*), which can be computed using DFT calculated HBE[105], is the key descriptor of HER activity. Therefore, calculations of HBE would allow us to evaluate the ΔG_H*, which in turn can be used to predict the HER activity of the catalysts qualitatively. Using this approach, the DFT calculations are performed to calculate the HBE on the stable Pt/Pd-ML-TMN(111) surfaces (Figure 4) to obtain ΔG_H*. All four adsorption sites: 2-hollow (fcc and hcp), 1 top and 1 bridge as shown in Figure 2 are considered for the calculations of HBE. The optimized DFT structures show that the fcc hollow site is the most favorable site for the adsorption of hydrogen on Pt/CrN, Pd/TaN, Pd/ZnN, while the most favorable site is hcp hollow for Pt/FeN, Pt/HfN, Pt/MnN, Pt/TiN, Pt/VN, Pd/CuN, Pd/CrN, Pd/FeN, Pd/HfN, Pd/MnN, Pd/NbN, Pd/ScN, Pd/TiN, Pd/VN, and Pd/ZrN.

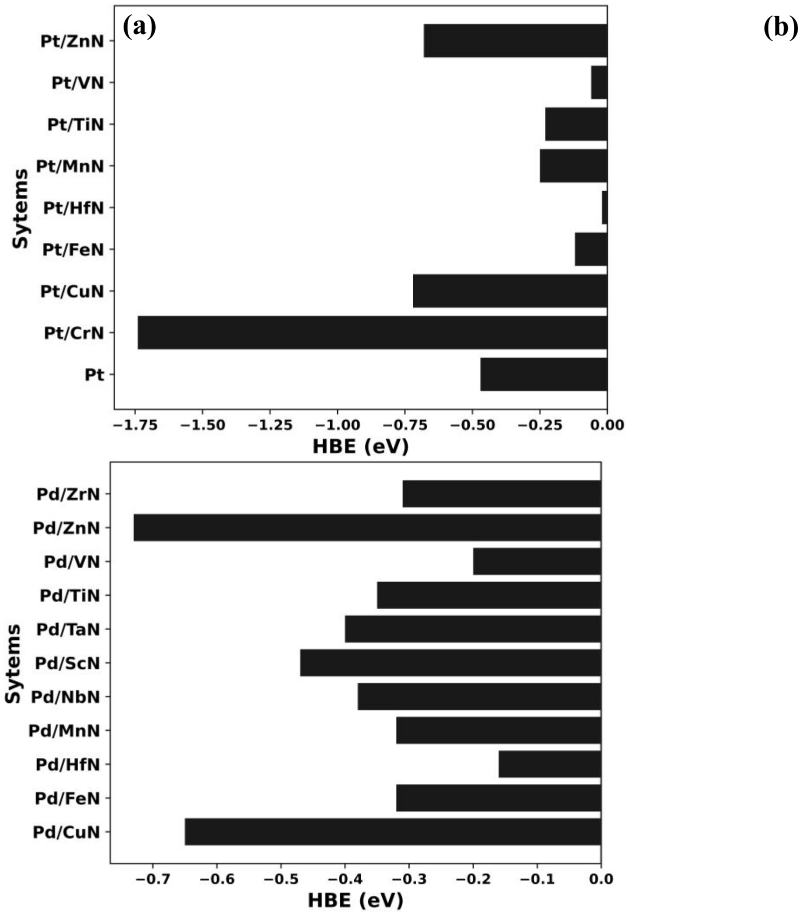

Figure 4. DFT calculated HBEs (in eV) on (a) Pt/TMN(111) and (b) Pd/TMNs(111) surfaces.

We find that the H binding on CrN, CuN, and ZnN is stronger than on Pt(111), while the H adsorption is weaker on FeN, HfN, MnN, TiN, and VN compared to Pt(111). Similarly, the H binding on Pd/CuN and Pd/ZrN is stronger than on Pt(111), while the H adsorption is weaker on Pd/FeN, Pd/HfN, Pd/MnN, Pd/NbN, Pd/TaN, Pd/TiN, Pd/VN, and Pd/ZrN compared to Pt(111). The H binding energy on Pd/ScN is similar to that on Pt(111).

The DFT calculated HBEs are then used to compute the ΔG_H* as described in equation 5 and the results are plotted as shown in Figures 5(a) and 5(b). Our computed ΔG_H* values in Figure

5(a) show that Pt/MnN and Pt/TiN have ΔG_H* close to zero (0.003 eV and 0.02 eV, respectively) and are predicted to be the best catalysts. The most difficult step of HER on Pt/MnN is desorption of *H (i. e.*H $\rightarrow 1/2H_2(g)$ + *: Tafel reaction) while the most difficult step of HER on Pt/TiN is Pt/TiN is H adsorption (i. e. $H^+ + e^- \rightarrow {}^*H$: Volmer reaction). On Pt/FeN, Pt/HfN, and Pt/VN the ΔG_H* values are calculated to be 0.13 eV, 0.23 eV, and 0.19 eV, respectively. These values are similar to or smaller than that on Pt (ΔG_H* = 0.22 eV), the best performing HER catalyst.[106-108] It is to be noted that the most difficult step of HER on Pt/FeN, Pt/HfN, and Pt/VN is the adsorption of H. The DFT calculations predict large ΔG_H* of 1.50 eV, 0.47 eV, and 0.43 eV on Pt/CrN, Pt/CuN, and Pt/ZnN, respectively. Thus, the HER is predicted to be sluggish on these candidates because of the associated large free energy barriers. The most difficult step of HER on Pt/CuN, Pt/CrN, and Pt/ZnN is found to be the desorption of H.

Similarly, DFT calculations are performed to compute the ΔG_H* values on Pd/TMNs. The free energy plots in Figure 5b show the ΔG_H* values are comparable or even smaller on Pd/VN (0.05 eV), Pd/ZrN (0.06 eV), Pd/MnN (0.07 eV), Pd/HfN (0.09 eV), Pd/TiN (0.10 eV), Pd/NbN (0.13 eV), and Pd/TaN (0.16) than on Pt(111). Thus, these candidates are predicted to show an excellent HER activity. Notably, the small (close to zero ΔG_H*) value observed on Pd/ZrN (0.06 eV), Pd/VN (0.05 eV) suggests that Pd/ZrN, Pd/VN should show superior HER performance. *H adsorption is predicted to be the rate-limiting step of HER on Pd/HfN, Pd/VN, while the desorption of H is found to be the most difficult step of HER on all other Pd/TMN. Our calculations show large ΔG_H* values of 0.81 eV, 0.48 eV and 0.40 eV on Pd/CrN, Pd/ZnN, and Pd/CuN, respectively. Therefore, a sluggish HER is predicted on Pd/CrN, Pd/ZnN and Pd/CuN.

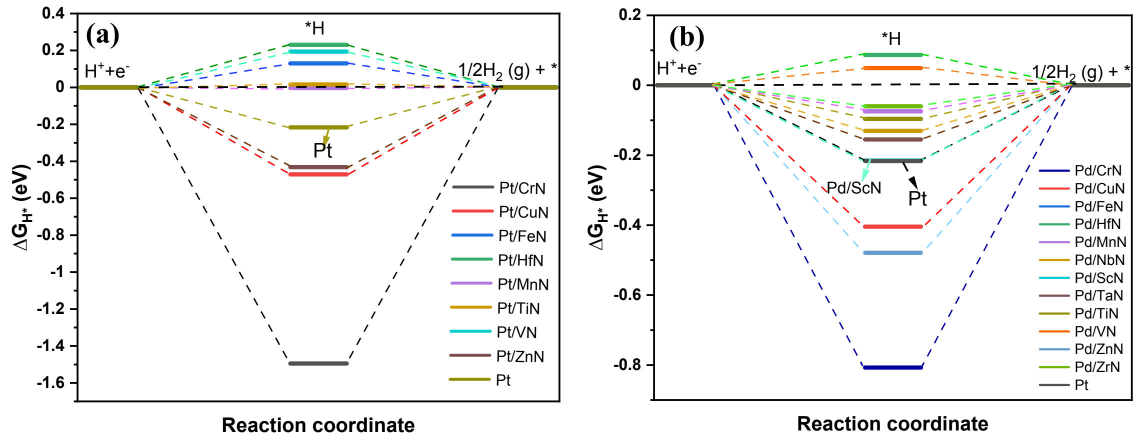

Figure 5. (a) DFT calculated free energy diagrams of HER at U = 0 V on (a) Pt/TMN(111) and (b) Pd/TMN(111).

Limiting potential (U_L), defined as the lowest applied potential (U) at which all elementary steps in free energy diagrams become downhill in energy, has been shown to correlate well with the catalytic activity of several electrochemical reactions, including the HER.[109] The DFT calculated ΔG_H* values are used to compute the U_L on Pt/Pd-ML-TMN(111). Subsequently, a plot of U_L and HBE on Pt/Pd ML on TMN(111) is constructed (Figure 6). The results show a volcano-like relationship between U_L and HBE. The U_L values on Pt/MnN, Pt/TiN, Pt/FeN, Pt/VN, Pt/HfN, Pt/ZnN, Pt/CuN, and Pt/CrN are -0.003 V, -0.02 V, -0.13 V, -0.19 V, -0.23 V, -0.43 V, -0.47 V, and -1.50 V, respectively. As shown in Figure 6, Pt/MnN and Pt/TiN lie at the top of the volcano and are predicted to be the best candidates among Pt/TMN sytsems. The calculated U_L values on Pt/FeN, Pt/HfN and Pt/VN are similar to Pt and are expected to show similar HER activity compared to Pt. The volcano plot in Figure 6 also shows that HBE is stronger on Pt/CrN, Pt/CuN and Pt/ZnN leading to a higher value of U_L.

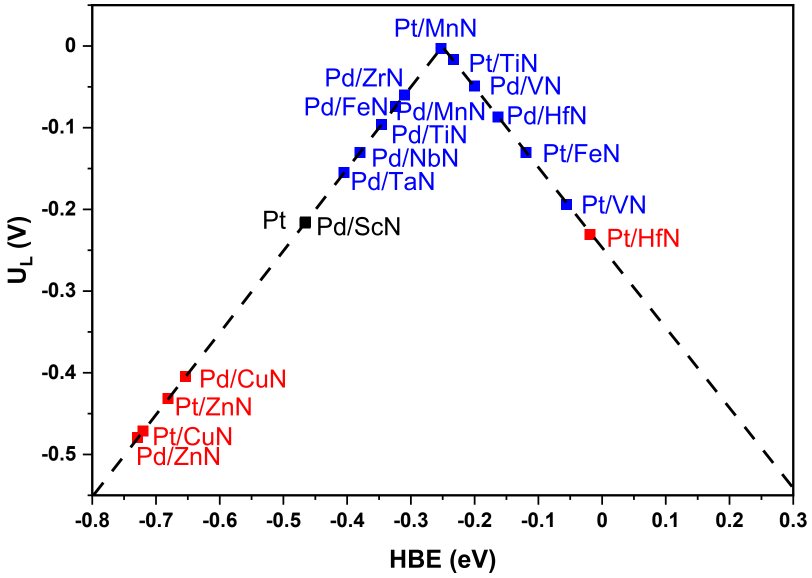

Figure 6. Correlation between U_L and HBE on Pt/TMNs and Pd/TMNs.

Similar volcano-like relationship is observed between U_L and HBE on Pd/TMNs. Figure 6 shows that Pd/ZrN and Pd/VN lie closest to the top of the volcano with U_L values of -0.06 V and -0.05 V, respectively. Pt and Pd/ScN both have U_L of -0.22 V. The U_L values are predicted to be -0.07 V, -0.09 V, -0.10 V, -0.13 V, and -0.16 V on Pd/MnN, Pd/HfN, Pd/TiN, Pd/NbN, and Pd/TaN, respectively. Pd/TaN, Pd/NbN, Pd/TiN, Pd/MnN, and Pd/HfN are predicted to show superior HER activity because of their smaller U_L values compared to Pt.

Figure 6 presents a correlation between U_L and HBE on Pt/TMN and Pd/TMN systems considered in this study. Pt/MnN and Pt/TiN lie at the top of the volcano, indicating that they efficiently catalyze the HER. The volcano-like relationship between U_L and HBE on Pt/Pd-ML-TMN(111) (Figure 6) illustrates that the candidates that have HBE in the range -0.47 eV and -0.06 eV should show enhanced HER activity compared to Pt. Thus, the future HER catalyst development efforts should focus on Pt/Pd-ML-TMN(111) candidates that have HBE in the range of -0.47 eV and -0.06 eV.

Finally, using the DFT method, we obtained the density of states (DOS) of surface Pt/Pd atoms on Pt/Pd-ML-TMN(111) and computed the d-band center as described elsewhere.[110] Our calculated d-band center shows a near-linear correlation with the HBE (Figure 7). The weaker HBE observed on Pt/Pd-ML-TMN(111) is due to the downshifting of the d-band center compared to Pt, while the upshift in the d-band center corresponds to the observed stronger HBE. The d-band centers of predicted best candidates are close to that of Pt, suggesting a similar HER activity of these candidates compared to Pt. In contrast, the d-band centers are significantly upshifted (compared to Pt) for the candidates such as Pt/CuN and Pd/ZnN making these candidates not ideal for enhanced HER. The observed linear correlation of HBE (which directly correlates with the activity of the catalysts) with the d-band center suggests that the d-band center can be used as a descriptor of HER activity on Pt/Pd-ML-TMN(111).

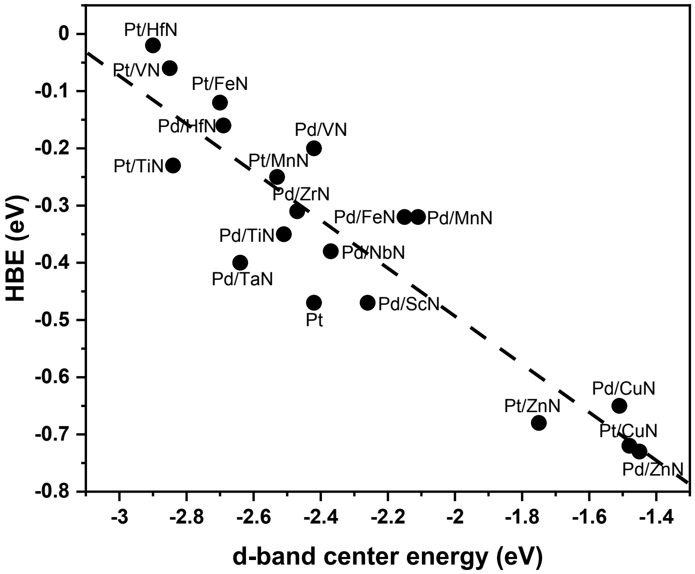

Figure 7. Plot showing the relationship between HBE (eV) and the d-band center (eV).

We performed AIMD simulations to test the thermal stability of DFT predicted two of the best candidates (Pd/VN and Pt/TiN). The results of AIMD simulations at 1000 K show a small fluctuation in the total energy (Figure 8). Importantly, we observed no significant buckling of Pt and Pd overlayers (geometries in Figure 8), indicating that Pd/VN and Pt/TiN remain stable up to 1000 K. Thus, the DFT predicted best candidates (e. g. Pt/TMN and Pd/TMN) are expected to be stable since the HER is typically carried out at ambient conditions with temperature ~300K.

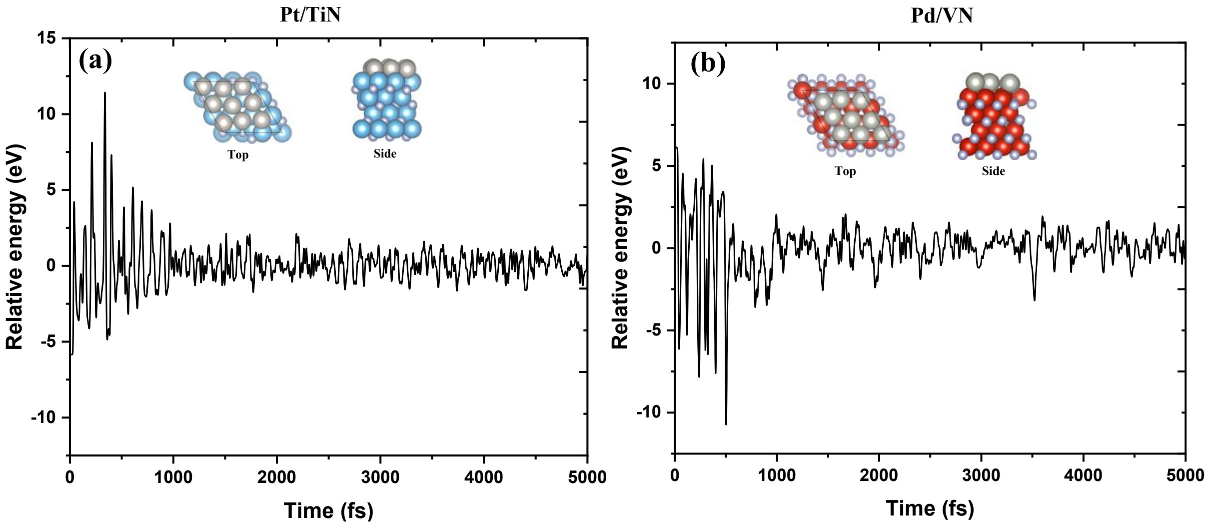

Figure 8. Fluctuation in total energy and snapshot of geometries (in inset) in AIMD simulations of (a) Pt/TiNi (b) Pd/VN at 1000 K.

4. CONCLUSIONS

We perform DFT calculations to investigate the HER activity of TMN@Pt/Pd core-shell catalyst structures modeled by Pt/Pd-ML-TMN(111) surfaces. The results show that several TMNs possess favorable negative formation energies as well as low surface energies for the formation of TMN(111) surfaces. Moreover, the strong binding between Pt/Pd with TM on TMN(111) suggests that Pt/Pd-ML-TMN(111) represents a promising catalyst structure for further exploration in catalysis. We carried out additional DFT calculations to compute the hydrogen binding energy (HBE) on Pt/Pd-ML-TMN(111). The DFT calculated HBEs are then used to compute the free energy change (ΔG_H*) along the HER pathway. Of all the Pt/Pd-ML-TMN(111), our results show that Pt/MnN, Pt/TiN, Pt/FeN, Pd/TaN, Pd/NbN, Pd/HfN, Pd/MnN, Pd/ScN, Pd/VN, and Pd/ZrN have ΔG_H* close to zero and have U_L values close to that of Pt(111). Thus, these candidates are predicted to show excellent HER activity. Furthermore, a volcano-type relationship between the DFT calculated HBE, and U_L suggests that the future HER catalyst development efforts should focus on Pt/Pd-ML-TMN(111) candidates that have HBE in the range of -0.47 eV and -0.06 eV.

ACKNOWLEDGEMENTS

This work was partially supported by NSF RIA (HRD 2055012) grant. The DFT calculations were performed using computational resources at the Extreme Science and Engineering Discovery Environment, which is supported by the National Science Foundation Grant number ACI-1548562. S. K. also acknowledges the faculty start-up fund from Florida A&M University.

REFERENCES

1. J. Zhu, L. Hu, P. Zhao, L.Y.S. Lee, and K. Wong, *Chem. Rev.*, 2020, 120, 851-918.
2. M. Cabán-Acevedo, M. L. Stone, J. R. Schmidt, J. G. Thomas, Q. Ding, H. C. Chang, M. L. Tsai, H. He and S. Jin, *Nat. Mater.*, 2015, 14, 1245–1251.
3. I. Staffel, D. Scamman, A.V. Abad, P. Balcombe, P.E. Dodds, P. Ekins, N. Shah, and K.R. Ward, *Energy Environ.,* 2019, 12, 463 -491.
4. P. Nikolaidis, A. Poullikkas, *Renew. Sust. Energ. Rev.,* 2017, 67, 597– 611.
5. D. Li, X. Li, and J. Gong, *Chem. Rev.* 2016, 116, 19, 11529-11653.
6. A. Ersoz, *Int J. Hydrog. Energy*, 2008, 33, 7084-7094.
7. S. Sengodan, R, Lan, J. Humphyreys, D. Du, W. Cu, H. Wang, and S. Tao, *Renew. Sust. Energ. Rev.*, 2018, 82, 761-780.
8. Q. Zhu, Y. Qu, D. Liu, K. W. Ng and H. Pan, *ACS Appl. Nano Mater.*, 2020, 3, 6270–6296.
9. F. Barbir*, Sol. Energy*, 2005, 78, 661–669.

10. S. A. Grigoriev, V. I. Porembsky and V. N. Fateev, in *Int. J. Hydrog. Energy*, 2006, vol. 31, pp. 171–175.

11. Z. Ge, B. Fu, J. Zhao, X. Li, B. Ma and Y. Chen, *J. Mater. Sci.*, 2020, 55, 14081–14104.

12. M. Wang, Z. Wang, X. Gong and Z. Guo, *Renew. Sustain. Energy Rev.*, 2014, 29, 573–588.

13. S. Shiva Kumar and V. Himabindu, *Mater. Sci. Energy Technol.*, 2019, 2, 442–454.

14. Z. Li, R. Ge, J. Su and L. Chen, *Adv. Mater. Interfaces*, 2020, 7.

15. S. Ye, C. Ding and C. Li, in *Adv Inorg Chem.*, 2019, vol. 74, pp. 3–59.

16. A. Züttel, A. Borgschulte and L. Schlapbach, *Hydrogen as a Future Energy Carrier*, 2008.

17. S. Wang, A. Lu and C. J. Zhong, *Nano Converg.*, 2021, 8.

18. Y. Cai, A. B. Anderson, J. C. Angus and L. N. Kostadinov, *J. Electrochem. Soc.*, 2007, 154, F36–F43.

19. S. Maheshwari, Y. Li, N. Agrawal and M. J. Janik, in *Adv. Catal.*, 2018, 63, 117–167.

20. M. T. Tang, X. Liu, Y. Ji, J. K. Norskov and K. Chan, *J. Phys. Chem. C*, 2020, 124, 28083–28092.

21. S. Bajracharya, A. ElMekawy, S. Srikanth and D. Pant, *in Microbial Electrochemical and Fuel Cells: Fundamentals and Applications*, 2016, 179–213.

22. D. Tian, S. R. Denny, K. Li, H. Wang, S. Kattel, and J.G. Chen, *Chem.Soc. Rev.*, 2021, 50, 12338.

23. S. Sarkar and S. C. Peter, *Inorg. Chem. Front.*, 2018, 5, 2060–2080.

24. H. Cheng, N. Yang, G. Liu, Y. Ge, J. Huang, Q. Yun, Y. Du, C. J. Sun, B. Chen, J. Liu and H. Zhang, *Adv. Mater.*, 2020, 32, 1902964.

25. F. Luo, Q. Zhang, X. Yu, S. Xiao, Y. Ling, H. Hu, L. Guo, Z. Yang, L. Huang, W. Cai and H. Cheng, *Angew. Chemie*, 2018, 130, 15078–15083.

26. R. Q. Yao, Y. T. Zhou, H. Shi, Q. H. Zhang, L. Gu, Z. Wen, X. Y. Lang and Q. Jiang, *ACS Energy Lett.*, 2019, 4, 1379–1386.

27. J. Sun, M. Ren, L. Yu, Z. Yang, L. Xie, F. Tian, Y. Yu, Z. Ren, S. Chen and H. Zhou, *Small*, 2019, 15, 1804272.

28. D. Y. Wang, M. Gong, H. L. Chou, C. J. Pan, H. A. Chen, Y. Wu, M. C. Lin, M. Guan, J. Yang, C. W. Chen, Y. L. Wang, B. J. Hwang, C. C. Chen and H. Dai, *J. Am. Chem. Soc.*, 2015, 137, 1587–1592.

29. J. Wang, W. Cui, Q. Liu, Z. Xing, A. M. Asiri and X. Sun, *Adv. Mater.*, 2016, 28, 215–230.

30. J. L. Kolar, *Environ. Qual. Manag.*, 2000, 10, 45–54.

31. D. Bhalothia, L. Krishnia, S. S. Yang, C. Yan, W. H. Hsiung, K. W. Wang and T. Y. Chen*,* *Appl. Sci.*, 2020, 10, 1–19.

32. B. H. R. Suryanto, Y. Wang, R. K. Hocking, W. Adamson and C. Zhao, *Nat. Commun.*, 2019, 10, 5599.

33. L. Cheng, W. Huang, Q. Gong, C. Liu, Z. Liu, Y. Li and H. Dai, *Angew. Chemie - Int. Ed.*, 2014, **53**, 7860–7863.

34. M. Shao, Q. Chang, JP Dodelet, R. Chenitz, *Chem Rev*, 2016, 116, 3594-3657.

35. Q. Zhang, Z. Jiang, BM Tackett, SR Denny, B. Tian, X. Chen, B. Wang, and JG Chen, *ACS. Catal.*, 2019, 9, 2415-2422.

36. R. Jiang, Z. Cui, W. Xu, S. Zhu, Y. Liang, Z. Li, S. Wu, C. Chang, A. Inoue *Electrochim. Acta*, 2019, 20, 135082.

37. S. S. Kumar, V. Himabindu, *Renew. Energy*, 2020, 146, 2281-2290.

38. S. K. Kim, Y. Qiu, Y. J. Zhang, R. Hurt and A. Peterson, *Appl. Catal. B Environ.*, 2018, 235, 36–44.

39. W. F. Chen, J. T. Muckerman and E. Fujita, *Chem. Commun.*, 2013, 49, 8896–8909.

40. Y. W. Cheng, J. H. Dai, Y. M. Zhang and Y. Song, *J. Phys. Chem. C*, 2018, 122, 28113–28122.

41. S. Meyer, A. V. Nikiforov, I. M. Petrushina, K. Köhler, E. Christensen, J. O. Jensen and N. J. Bjerrum, *Int. J. Hydrog. Energy*, 2015, 40, 2905–2911.

42. D. Jin, L. R. Johnson, A. S. Raman, X. Ming, Y. Gao, F. Du, Y. Wei, G. Chen, A. Vojvodic, Y. Gogotsi and X. Meng, *J. Phys. Chem. C*, 2020, 124, 10584–10592.

43. C. Yang, R. Zhao, H. Xiang, J. Wu, W. Zhong, W. Li, Q. Zhang, N. Yang and X. Li, *Adv. Energy Mater.*, 2020, 10, 2002260

44. Q. Zhang, Z. Jiang, B. M. Tackett, S. R. Denny, B. Tian, X. Chen, B. Wang and J. G. Chen, *ACS Catal.*, 2019, 9, 2415–2422.

45. J. Xie and Y. Xie, *Chem. - A Eur. J.*, 2016, 22, 3588–3598.

46. B. Cao, G. M. Veith, J. C. Neuefeind, R. R. Adzic and P. G. Khalifah, *J. Am. Chem. Soc.*, 2013, 135, 19186–19192.

47. J. Theerthagiri, S. J. Lee, A. P. Murthy, J. Madhavan and M. Y. Choi, Curr. Opin. *Solid State Mater. Sci.*, 2020, 24.

48. W. Qi, Y. Zhou, S. Liu, H. Liu, L. S. Hui, A. Turak, J. Wang and M. Yang, *Appl. Mater. Today*, 2019, 100476.

49. H. Du, R. M. Kong, X. Guo, F. Qu and J. Li, *Nanoscale*, 2018, 10, 21617–21624.

50. S. M. El-Refaei, P. A. Russo and N. Pinna, *ACS Appl. Mater. Interfaces*, 2021.

51. T. W. Wang, T. L. Wang, W. J. Chou, L. F. Wu and S. H. Lin, *Phys. Chem. Chem. Phys.*, 2021, 23, 2305–2312.

52. X. Lv, Z. Hu, H. Zhao, Y. Liu and Z. Yuan, *Prog. Chem.*, 2018, 30, 947–957.

53. X. Liu, X. Ge, Y. Dong, K. Fu, F. Meng, R. Si, M. Zhang and X. Xu, Mater. *Chem. Phys.*, , 2020, 253, 123334.

54. Y. Abghoui and E. Skúlason, *J. Phys. Chem. C*, 2017, 121, 24036–24045.

55. Y. Liu, D. Tian, A. N. Biswas, Z. Xie, S. Hwang, J. H. Lee, H. Meng, J. G. Chen Angew. Chem. Int. Ed., 2020, 59, 11345-11348.

56. S. Dutta, A. Indra, Y. Feng, H. Han, T. Song, Appl. Catal. B., 241, 2019, 521-527.

57. S. A. Raheem, H. Shen, T. Thomas and M. Yang, Phys. Chem. Chem. Phys., 2022,24, 771-777.

58. R. Zhang, Y. Zhang, X. Ren, G. Cui, A. M. Asiri, B. Zheng, and X. Sun, ACS Sustain. Chem. Eng, 2018, 6, 9545-9549.

59. X. Yang, S. Kattel, J. Nash, X. Chang, J. H. Lee, Y. Yan, J. G. Chen, B. Xu, Angew. Chem. Int. Ed., 2019, 58, 13768-13772.

60. M. Yang, Z. Cui, F.D. DiSalvo, Phys. Chem. Chem. Phys.,2013, 15, 1088.

61. K. R. Yoon, K. Shin, J. Park, S. Cho, C. Kim, J. Jung, J. Y. Cheong, H. R. Byon, H. M. Lee, and I. Kim, ACS Nano 2018 12 (1), 128-139.

62. T. Wu, X. Wang, A. E. Emre, J. Fan, Y. Min, Q. Xu, S. Sun, L. Energy Chem, 2021, 55, 48-54.

63. R. Michalsky, Y. J. Zhang and A. A. Peterson, *ACS Catal.*, 2014, 4, 1274–1278.

64. G. Kresse and J. Furthmüller, *Comput. Mater. Sci.*, 1996, 6, 15–50.

65. K. G. and H. J., *Phys. Rev. B*, 1993, 48, 48–51.

66. S. Equations and C. Effects, *Phys. Rev.*, 1965, 140, 1133–1138.

67. P. E. Bloch, *Phys. Rev. B*, 1994, 50, 17953–17979.

68. J. P. Perdew and Y. Wang, *Phys. Rev. B*, 1992, 46, 12947–12954.

69. D. J. Chadi, *Phys. Rev. B*, 1977, 16, 1746–1747.

70. Q. Chang, J.H Lee, Y. Liu, Z. Xie, S. Hwang, N.S. Marinkovic, A. A. Park, S. Kattel, J. G. Chen, JACS Au, 2, 214-222.

71. Z. Xie, Y. Xu, M. Xie, X. Chen, H. H. Lee, E. Stavitski, S. Kattel, J. G. Chen, Nat. commun., 2020, 11, 1-8.

72. J. Wang, S. Kattel, C. J. Hawxhurst, J.H. Lee, B. M. Tackett, K. Chang, N. Rui, C. Liu, J. G. Chen, Angewandte Chemie International Edition, 2019, 58 (19), 6271-6275.

73. M. G. Quesne, A. Roldan, N. H. De Leeuw and C. R. A. Catlow, *Phys. Chem. Chem. Phys.*, 2018, 20, 6905–6916.

74. J. K. Nørskov, J. Rossmeisl, A. Logadottir, L. Lindqvist, J. R. Kitchin, T. Bligaard and H. Jónsson, *J. Phys. Chem. B*, 2004, 108, 17886–17892.

75. F. Li and Q. Tang, ACS Appl. Nano Mater. 2019, 2, 7220−7229.

76. Y. Nian, Y. Wang, A. N. Biswas, X. Chen, Y. Hou, J. G. Chen, Chem. Eng. J., 2021, 426, 130781.

77. Z. Lin, S. R. Denny, J. G. Chen, Journal of Catalysis, 2021, 404, 929-942.

78. D. Tian, S. R. Denny, K. Li, H. Wang, S. Kattel, and J. G. Chen Chem. Soc. Rev., 2021,50, 12338-12376.

79. Q. Zhang, Z. Jiang, B. M. Tackett, S. R. Deeny, B. Tian, X. Chen, B. Wang, and J. G. Chen, ACS Catalysis 9 (3), 2415-2422.

80. Z. Lin, R. Chen, Z. Qu, and J. G. Chen, Green chemistry 20 (12), 2679-2696.

81. Z. Lin, S. C. Ammal, S. R. Denny, S. A. Rkov, K. You, A. Heyden, and J. G. Chen, JACS Au 2022, 2, 2, 367–379.

82. Y. Liu, D. Tian, A. N. Biswas, Z. Xie, S. Hwang, J. H. Lee, H. Meng, and J. G. Chen, Angew. Chem. Int. Ed., 2020, 59, 11345-11348.

83. Y. Sun, B. Yao, Q. He, F. Su, and H. Z. Wang, J. Alloys Compd., 2009, 479, 599-602.

84. S. Wang, X. Yu, J. Zhang, L. Wang, K. Leinenweber, D. He, and Y. Zhao, Cryst. Growth Des. 2016, 16, 1, 351–358.

85. A. A. Barragan, N. V. Ilawe, L. Zhong, B. M. Wong, and L. Mangolini, J. Phys. Chem. C, 2017, 121, 4, 2316–2322.

86. M. G. Moreno-Armenta, J. Diaz, A. Martinez-Ruiz, and G. Soto, J. Phys. Chem. Solids 2007, 68, 1989-1994.

87. X. Liu, H. Lu, M. He, K. Jin, G. Yang, H. Ni, and K. Zhao, J. Alloys Compd. 2014, 582, 75-78.

88. D. Ologunagba and S. Kattel, *Energies*, 2020, 13, 2182.

89. D. V. Esposito, S. T. Hunt, Y. C. Kimmel, and J. G. Chen, J. Am. Chem. Soc. 2012, 134, 3025–3033.

90. J. L. R. Yates, G. H. Spikes, and G. Jones, Phys. Chem. Chem. Phys., 2015,17, 4250-4258.

91. J. Dong, Q. Fu, Z. Jiang, B. Mei, and X. Bao, J. Am. Chem. Soc. 2018, 140, 42, 13808–13816.

92. H. H. Hwu and J. G. Chen, *Chem. Rev.*, 2005, 105, 185-212.

93. B. Liu, L. Huo, R. Si, J. Liu, J. Zhang, *ACS Appl. Mater. Interfaces*, 2016, 18770-18787

94. D. Göhl, A. Garg, P. Paciok, KJJ, Mayrhofer, M. Heggen, Y. Shao-Horn, RE, Dunin-Borkowski, Y. Román-Leshkov, M. Ledendecker *Nat. Mater.* 2020, 19, 287–291.

95. S. T. Hunt, and M. Milina, A. C. Alba-Rubio, C. H. Hendon, J. A. Dumesic, and Y. Román-Leshkov, *Science*, 2016, 352, 974-978.

96. A. Garg, M. Milina, Prof. D. Zanchet, and S. T. Hunt, *Angew.Chem. Int. Ed.*, 2017, 56, 8828 –8833.

97. S. T. Hunt, M. Milina, Z. Wang, and Y. Roman-Leshkov, *Energy Environ. Sci.*, 2016, 9, 3290–3301.

98. C. Kura, Y. Kunisada, E. Tsuji, C. Zhu, H. Habazaki, S. Nagata, M. P. Muller, R. A. De Souza, and Y. Aoki, *Nat. Energy*, 2017, 2, 786–794.

99. N. A. Koratkar, *Nat. Mater.*, 2016 15, 1153–1154.

100. H. J. Yan, C. Tian, L. Wang, A. Wu, M. Meng, L. Zhao, and H. Fu., *Angew. Chem. Int. Ed.*, 2015, 54, 6325–6329.

101. H. Guan, W. Li, J. Han, W. Yi, H. Bai, Q. Kong, and G. Xi., *Nat Commun*, 2021, 12, 1376.

102. A. B. Laursen, A. S. Varela, F. Dionigi, H. Fanchiu, C. Miller, O. L. Trinhammer, J. Rossmeisl, and S. Dahl, *J. Chem. Educ.*, 2012, 89, 1595-1599.

103. Kai S. Exner, *Curr Opin Electrochem.*, 2021, 26, 2451-9103.

104. M. T. M. Koper and E. Bouwman, *Angew.Chem. Int. Ed.*, 2010, 49, 3723 – 3725.

105. Q. Zhang, Z. Jiang, B.M. Tackett, S. R. Denny, B. Tian, X. Chen, B. Wang and J. G. Chen, *ACS Catal.*, 2019, 9, 2415-2422.

106. N. Cheng, S. Stambula, D. Wang, M. N. Banis, J. Liu, A. Riese, B. Xiao, R. Li, T. Sham, L. Liu, G. A. Botton, and X. Sun, *Nat Commun,* 2016, 7, 13638.

107. C. Li and J. Baek, *ACS Omega*, 2020, 5, 31-40.

108. B. Ruqia, and S.-I. Choi, *ChemSusChem*, 2018, 11, 2643−2653.

109. A. Kulkarni, S. Siahrostami, A. Patel, and JK. Norskov, *Chem. Rev.*, 2018, 118, 2302-2312.

110. A. Vojvodic, J. K. Nørskov, F. Abild-Pedersen, *Top Catal.*, 2014, 57, 25–32.